Published in final edited form as:
Nat Med. 2015 June ; 21(6): 591–600. doi:10.1038/nm.3856.

Metabolic regulation of hepatitis B immunopathology by myeloid-derived suppressor cells

Laura J. Pallett[1], **Upkar S. Gill**[2], **Alberto Quaglia**[3], **Linda V. Sinclair**[4], **Maria Jover-Cobos**[5], **Anna Schurich**[1], **Kasha P. Singh**[1], **Niclas Thomas**[1], **Abhishek Das**[1], **Antony Chen**[1], **Giuseppe Fusai**[5], **Antonio Bertoletti**[6,7], **Doreen A. Cantrell**[4], **Patrick T. Kennedy**[2], **Nathan A. Davies**[5], **Muzlifah Haniffa**[7,8], and **Mala K. Maini**[1]

[1]Division of Infection and Immunity and Institute of Immunity and Transplantation, University College London, London, UK

[2]Centre for Digestive Diseases, Blizard Institue, Bart's and the London School of Medicine and Dentistry, London, UK

[3]Institute of Liver Studies, Kings College Hospital, London, UK

[4]Division of Cell Signaling and Immunology, University of Dundee, Dundee, UK

[5]Institute of Liver and Digestive Health, University College London, London, UK

[6]Duke-Nus Medical School, Emerging Infectious Disease Program, Singapore

[7]Singapore Institute for Clinical Sciences, Agency of Science and Technology, Singapore

[8]Institute of Cellular Medicine, Newcastle University, UK

Abstract

Infection with hepatitis B virus (HBV) results in disparate degrees of tissue injury: it can replicate without pathological consequences or trigger immune-mediated necroinflammatory liver damage. We investigated the potential for myeloid-derived suppressor cells (MDSC) to suppress T cell-mediated immunopathology in this setting. Granulocytic MDSC (gMDSC) expanded transiently in acute resolving HBV, decreasing before peak hepatic injury. In persistent infection, arginase-expressing gMDSC (and circulating arginase) increased most in phases characterized by HBV replication without immunopathology, whilst L-arginine decreased. gMDSC expressed liver-homing chemokine receptors and accumulated in the liver, their expansion being supported by hepatic stellate cells. We provide *in vitro* and *ex vivo* evidence that gMDSC potently inhibited T cells in a partially arginase-dependent manner. L-arginine-deprived T cells upregulated system-L amino acid transporters to increase uptake of essential nutrients and attempt metabolic

Corresponding author: Mala K. Maini, Division of Infection and Immunity, University College London, Rayne Building, 5 University Street, London, WC1E 6JF., Tel: +44 (0)20 3108 2170, Fax: +44 (0)20 3108 2119, m.maini@ucl.ac.uk.

Author Contributions

LJP, AB, MH, MKM conceived the project, LJP, AQ, LVS, MJ-C, KPS, AD, AB, DAC, ND, MH, MKM designed the experiments; LJP, AQ, LVS, MJ-C, KPS, NT, AC, MH generated data; LJP, UG, AQ, LVS, AS, KPS, NT, ND, MKM analyzed data; UG, GF, PTK provided essential patient samples; LJP and MKM prepared the manuscript, UG, AQ, LVS, AS, KPS, NT, AD, AC, GF, AB, DAC, PTK, ND, MH provided critical review of the manuscript.

Europe PMC Funders Author Manuscripts

reprogramming. These data demonstrate the capacity of expanded arginase-expressing gMDSC to regulate liver immunopathology in HBV infection.

Immune responses in the liver are tightly regulated to preserve the integrity of this vital organ. Hepatotropic viruses such as HBV exploit the tolerogenic environment in the liver to establish persistent infection in around 350 million people worldwide. HBV is a non-cytopathic virus; the liver disease it triggers, resulting in cirrhosis and hepatocellular carcinoma, is immune-mediated[1]. HBV can elicit starkly contrasting outcomes, recognized as distinct clinical phases; replicating at extremely high levels for decades without clinically apparent liver disease ("immunotolerant" phase), or, in contrast, driving a marked necroinflammatory reaction (active liver disease). The immune mechanisms distinguishing these phases, and the transition between them, have not been established.

In chronic HBV infection (CHB), an inadequate HBV-specific T cell response can trigger a large non-antigen-specific cellular infiltrate, amplifying liver damage through bystander T cells[1-5]. Here we have explored how such responses are blunted in phases when there is ongoing viral replication without overt liver inflammation, as a paradigm of immunoregulation of tissue damage. We previously noted a proliferative defect in global T cell responses in CHB accompanied by CD3-ζ-chain downregulation, a hallmark of L-arginine deprivation[6]. We therefore postulated that nutrient deprivation might be a factor limiting T cell responses in the metabolically restricted environment of the liver. Recent data highlight the central role of the metabolic milieu in regulating immunity, with an increased requirement for amino acids imposed by the demands of mounting an effective immune response[7,8].

A cell type increasingly recognized to exert potent immunoregulation through metabolic manipulation is the myeloid-derived suppressor cell (MDSC). These immature myeloid cells expand in tumor infiltrates, down-regulating local and systemic immune responses by, for example, production of arginase I, which catabolizes L-arginine to deprive immune effectors of this amino acid[9]. Emerging data also implicate MDSC in inhibiting antiviral immunity[10-13] but their potential for regulating amino acid metabolism has not been examined in individuals with HBV infection.

In this study we demonstrate expansion of the granulocytic subset of MDSC (gMDSC) in subjects sustaining HBV replication without necroinflammatory liver disease. Our data indicate that this protective effect may be mediated by the capacity of gMDSC expressing arginase I to potently inhibit T cell responses. Our findings highlight the capacity of gMDSC to moderate tissue damage in a common human infection by constraining nutrient supplies to proliferating T cells.

Results

gMDSC expansion in subjects with HBV replication without liver damage

Circulating frequencies of gMDSC were quantified with the gating strategy indicated (Fig. 1a), using freshly isolated samples since gMDSC are cryo-sensitive (Supplementary Fig.

1a)[14]. Flow cytometric identification of CD66b and CD16 and cytospin staining confirmed the granulocytic nature of the gMDSC population analyzed (Supplementary Fig. 1b-c)[15,16].

The frequency of gMDSC was increased (mean 8-fold, maximum 20-fold) in a cohort of 84 subjects with CHB (Supplementary Table I) compared to 44 healthy controls (as percentage of myeloid cells Fig. 1b, absolute numbers Supplementary Fig. 1d). This finding was reproducible in a separately sampled cohort (54 CHB, 55 healthy controls), although gMDSC frequencies were proportionately decreased in this cohort, attributable to collection of blood in EDTA versus heparin (Supplementary Fig. 1e).

In some patients with CHB, the expanded population of gMDSC accounted for as much as 45% of circulating myeloid cells (Fig. 1b), whereas the monocytic subset of MDSC (mMDSC) was not significantly increased (Fig. 1c). The percent of gMDSC in CHB was highly variable (Fig. 1b, Supplementary Fig. 1e), with the spread not attributable to age or cytomegalovirus (CMV) serostatus (Supplementary Fig. 1f-g). However females with CHB (known to develop less HBV-related liver inflammation[17]) had higher frequencies of gMDSC than males (Fig. 1d). Examining virological parameters, gMDSC numbers did not correlate significantly with viral load, serum HBsAg titer or HBeAg status (Supplementary Fig. 1h-j); no interdependent relationship between these variables was detected using multiple linear regression or principal component analysis (data not shown).

HBV is a non-cytopathic virus, with disease activity attributed to the degree of immunopathology rather than viral replication. We therefore analyzed gMDSC frequencies in a subset of the cohort who could be classified by repeated assessment of clinical parameters into four major phases of disease activity: “immunotolerants”, “$HBeAg^+$ active disease”, “inactive disease”, “$HBeAg^-$ active disease” (diagnostic cut-offs defined in Fig. 1e legend). Donors sustaining HBV replication in the absence of liver inflammation (assessed by repeated serum alanine transaminase (ALT) quantitation) had significantly higher gMDSC frequencies (Fig. 1e) and absolute numbers (data not shown) than those with active liver disease.

In 42 individuals, liver biopsy tissue was available for histological assessment of immune-mediated pathology; the percentage of gMDSC correlated inversely with their hepatic necroinflammatory score (Fig. 1g). These findings were concisely displayed via hierarchical clustering by Euclidean distance (Fig. 1h). Clustering in an unsupervised manner based on similarity of ALT, necroinflammatory score and gMDSC frequencies showed that a high frequency of gMDSC was concordant with low ALT and necroinflammatory score. Immunotolerant and inactive disease clustered together, with $HBeAg^+$ and $HBeAg^-$ active disease forming a separate cluster. Taken together, these data implicate a role for gMDSC in protecting against liver disease in CHB.

Temporal dynamics of gMDSC frequencies in acute and chronic HBV flares

To further dissect the relationship between HBV disease activity and gMDSC, we analyzed their frequency during the dynamic changes characterizing acute infection in three individuals who, unusually, had been sampled from the initial pre-clinical phase until disease resolution. We confirmed that although gMDSC are reduced by cryopreservation,

they remain in direct proportion to their *ex vivo* frequency (Supplementary Fig. 1a), allowing valid interpretation of longitudinal trends within these cryopreserved samples. In the two donors sampled before or at peak viremia, a clear temporal correlation between increases in gMDSC and HBV load was observed, with these parameters subsequently decreasing in parallel (Fig. 2a as percentage of myeloid, Supplementary Fig. 2a as percentage of live leukocytes).

Subjects showed the delay between peak viremia and subsequent hepatic flare (measured by ALT increases to >2000 IU/L) characteristic of acute HBV. Analogous to our cross-sectional findings in chronic infection, gMDSC frequencies correlated inversely with ALT; highest when there was high-level viral replication without liver damage, and decreasing when the acute flare of hepatic injury peaked (Fig. 2b as percentage of myeloid, Supplementary Fig. 2b as percentage of live leukocytes). Samples obtained during the intermittent, spontaneous hepatic flares characteristic of $HBeAg^-$ chronic disease likewise showed a close inverse temporal relationship between liver inflammation and gMDSC frequencies (Fig. 2c as percentage of myeloid, Supplementary Fig. 2c as percentage of live leukocytes).

These findings are in line with data from the mouse lymphocytic choriomeningitis virus (LCMV) model, showing transient expansion of MDSC during acute infection, contrasting with their more sustained expansion during persistent infection[10]. Our results provide direct *ex vivo* evidence for the expansion of human gMDSC in acute HBV infection and their inverse temporal correlation with hepatic flares, further suggesting that they may suppress liver inflammation.

Degranulating arginase$^+$ gMDSC in CHB without immunopathology

We next tested the postulate that gMDSC could suppress inflammation in CHB through the production of the enzyme arginase I. gMDSC, along with low density neutrophils, were the only circulating cell subsets showing strong staining for arginase I (Fig. 3a, Supplementary Fig. 3a), with consistently greater intensity than mMDSC (Supplementary Fig. 3b). Subjects with CHB had a high proportion of gMDSC expressing arginase I (mean ± SEM, 81.2 ± 3.2%, data not shown). There was a marked increase in the proportion of arginase$^+$ gMDSC circulating in CHB compared to controls (Fig. 3b), particularly in the immunotolerant and inactive phases of CHB (Fig. 3c).

Imagestream analysis showed a granular pattern of distribution of arginase I throughout gMDSC (Supplementary Fig. 3c). Surface expression of CD63 was increased on gMDSC in CHB compared to healthy controls (Supplementary Fig. 3d), indicative of an enhanced capacity to degranulate and release arginase I[18,19]. Serum arginase I was also increased in patients with CHB compared to controls (Fig. 3d), and correlated with gMDSC frequency (Fig. 3e), in line with this population being a major source of circulating arginase I. The preferential expansion of arginase$^+$ gMDSC in the immunotolerant phase was mirrored by increased circulating arginase I concentrations in this group (Fig. 3f), and reflected in the inverse correlation between serum arginase I and ALT (Fig. 3g, Supplementary Fig. 3e).

Ex vivo evidence of selective L-arginine depletion in CHB

To corroborate the functionality of arginase^{+} gMDSC, we used tandem high-performance liquid chromatography mass spectrometry to quantitate L-arginine, the amino acid substrate of arginase I. Consistent with their expanded population of arginase^{+} gMDSC, individuals with CHB, particularly those without liver inflammation, had lower serum concentrations of L-arginine than healthy controls (Fig. 3h, Supplementary Fig. 3f). L-tryptophan, also implicated in immune regulation[20], showed a non-significant trend to decrease in CHB (Supplementary Fig. 3g), whereas L-phenylalanine did not differ (Supplementary Fig. 3h).

To further probe the contribution of HBV infection to the gMDSC-dependent depletion of L-arginine, we obtained samples from 7 individuals before and during antiviral therapy. We observed that L-arginine levels were partially restored in 5 out of 7 patients once HBV replication was suppressed by antivirals (Fig. 3i), the degree of L-arginine increase robustly correlating with the extent of disease suppression (Fig. 3j).

Accumulation of arginase^{+} gMDSC in the liver

We next investigated whether the expanded population of gMDSC circulating in subjects with CHB could home to the liver to regulate inflammation at the site of HBV replication. Simultaneous quantitation of gMDSC from paired blood and surplus liver biopsy tissue from 36 subjects with CHB showed that gMDSC accumulated in the liver (maximum 56% of intrahepatic myeloid cells Fig. 4a, and 9% of total live liver cellular extracts Supplementary Fig. 4a). By contrast, mMDSC were reduced in the intrahepatic compartment (Supplementary Fig. 4b). Samples from a cohort of individuals with chronic HCV infection revealed that another hepatotropic viral infection could also drive the expansion of gMDSC in the blood and enrichment in the liver compartment (Supplementary Fig.4c-d).

In individuals with CHB, intrahepatic gMDSC expressed more arginase I and surface CD63 than their circulating counterparts (Fig. 4b-c), consistent with an enhanced potential to release arginase I and mediate immunosuppression by L-arginine depletion within the liver. Arginase I levels were markedly increased in gMDSC compared to other cellular fractions in liver extracts (Supplementary Fig. 4e). An additional potential source of arginase I is necrotic hepatocytes, but this has low extracellular stability due to rapid loss of divalent metal ions and requires an alkaline pH for full activity[21-23] (Supplementary Fig. 4f). In contrast, arginase^{+} gMDSC co-express azurophilic granules (identified by their expression of myeloperoxidase (MPO), Supplementary Fig. 4g), that can release a factor critical for activating arginase I at physiological pH[24].

We then stained circulating gMDSC for chemokine receptors potentially relevant to their mobilization or liver-homing, based on recent studies[25]. CCR2, critical for the mobilization of MDSC from the bone marrow in LCMV[10], was expressed at high levels on mMDSC but barely detectable on gMDSC (Fig. 4d). Loss of signaling through another chemokine receptor, CXCR4, promotes the egress of immature granulocytes from the bone marrow[26,27]; CXCR4 was expressed at reduced levels on gMDSC in CHB (Fig. 4d), suggesting its downregulation may have accelerated their mobilization. Expression of CXCR3 was markedly increased on gMDSC in the liver compared to the circulation (Fig.

4e, Supplementary Fig. 4h), whilst CXCR1 was expressed at high levels by circulating and intrahepatic gMDSC (Fig. 4f, Supplementary Fig. 4i), potentially allowing them to interact with hepatic stellate cells, that can produce the chemotactic cytokine IL-8[28].

Hepatic stellate cells are specialized, liver-resident stromal cells, recently reported to be able to support the expansion of MDSC[29-31]. We isolated and cultured primary hepatic stellate cells (pHSC) from healthy resected liver tissue and found they increased the expansion of gMDSC in PBMC from controls or subjects with CHB (Fig. 4g). Taken together, these data suggest that downregulation of CXCR4 may favor the egress of gMDSC from the bone marrow into the circulation in CHB, whilst their accumulation in the liver could be directed by their expression of CXCR3 and CXCR1, and supported by pHSC. Their potential to interact with pHSC was underscored by visualizing gMDSC within the liver sinusoids in sections from HBV-infected livers, where they were also forced into close proximity with infiltrating T cells (Fig. 4h-i).

gMDSC suppress HBV-specific and bystander T cell responses

To investigate whether gMDSC had the potential to suppress the T cells they encounter in the liver, we tested their impact on the expansion of HBV-specific T cells in co-culture. HBV-specific T cell IFN-γ responses were rescued by depletion of gMDSC (Fig. 5a and Supplementary Fig. 5a). Conversely, HBV-specific $CD4^+$ and $CD8^+$ T cell responses were almost completely abrogated by the addition of gMDSC (Fig. 5a-b).

We next sought functional evidence that L-arginine deprivation by gMDSC could suppress bystander T cell responses, that play a crucial role in amplifying HBV-related immunopathology in mouse models and human disease[1,3]. To investigate this we analyzed subjects with CHB for pooled influenza, Epstein-Barr virus (EBV) and CMV-specific T cell responses. Again, removal of gMDSC increased expansion of peptide-specific IFN-γ^+ T cells, whereas their re-addition suppressed responses to these viruses in all donors (Fig. 5c-d), even at an effector:target ratio of 1 to 4 (Supplementary Fig. 5b).

Treatment of gMDSC with the specific arginase I inhibitor *N*-hydroxy-nor-L-arginine (nor-NOHA) reduced their suppressive activity, partially restoring T cell IFN-γ responses (Fig. 5e). Addition of nor-NOHA to PBMC produced marginal increases in responses, congruent with the lower frequency of arginase+ gMDSC (Fig. 5e). gMDSC could likewise suppress other $CD8^+$ T cell functions potentially contributing to liver damage (TNF-α and granzyme B) in an arginase-dependent manner (Supplementary Fig. 5c-d). T cells cultured with gMDSC showed downregulation of CD3-ζ and impaired proliferative capacity, hallmarks of L-arginine deprivation[6,32] (Supplementary Fig. 5e). gMDSC obtained by flow cytometry instead of bead-sorting (purity Supplementary Fig. 5f) similarly suppressed T cell cytokines and down-regulated CD3-ζ (Supplementary Fig. 5g).

To investigate the effect of gMDSC on T cells directly *ex vivo*, we examined the temporal changes in CD3-ζ (as a hallmark of L-arginine deprivation) in parallel with fluctuations in gMDSC frequencies over the course of acute and chronic flares of HBV disease. In all flaring patients in whom gMDSC had been quantitated longitudinally (Fig. 2), we observed a striking *ex vivo* inverse temporal relationship between numbers of gMDSC and CD3-ζ

expression on global T cells (Fig. 5f). These findings suggested that gMDSC could impede T cell responses capable of driving liver pathology by depleting their L-arginine supply.

L-arginine deprivation induces system-L amino acid transporters

Uptake of certain essential amino acids by T cells is dependent on the system-L amino acid transporters, that have recently been shown to play a critical role in the metabolic reprogramming required for a proliferative response to TCR-mediated signaling[7,33]. We therefore stained for CD98 on T cells to identify the family of system-L amino acid transporters (Slc7a5, Slc7a6, Slc7a7, Slc7a8) that form heterodimers with the CD98 heavy chain[7,34]. *Ex vivo* levels of CD98 on T cells were low, but were increased in some individuals with CHB compared to healthy controls (Fig. 6a, Supplementary Fig. 6a).

It has previously been shown that levels of Slc7a5 on rat hepatocytes can increase in response to L-arginine starvation[35]. We hypothesized that T cells infiltrating the extensive liver vasculature could be subjected to prolonged periods of L-arginine deprivation, manifested as a compensatory increase in Slc7a5 (and monitored by CD98 expression). To investigate this, paired blood samples and liver biopsy tissue from 11 individuals with CHB were used for the comparison of circulating and intrahepatic T cells. The number of T cells expressing CD98 directly *ex vivo*, and the level of their expression, was increased in the intrahepatic compared to circulating compartment in all patients examined (Fig. 6b, Supplementary Fig. 6b). We therefore investigated the expression of CD98 on HBV-specific $CD8^+$ T cells, which would have encountered their antigen in the liver milieu, identified directly *ex vivo* by HLA-A2/HBV-peptide multimer staining. HBV-specific $CD8^+$ T cells had significantly higher expression of CD98 than global $CD8^+$ T cells in all subjects examined (Fig.6c, Supplementary Fig. 6c). HBV-specific $CD8^+$ T cells also had consistently higher CD98 than their CMV-specific CD8 T cell counterparts in the same individuals (Fig. 6d, Supplementary Fig. 6d), which in turn had higher expression than the global population of $CD8^+$ cells in these subjects with CHB (Supplementary Fig. 6e).

To test whether the increases in CD98 we observed in intrahepatic and virus-specific T cells in CHB could represent a compensatory response to L-arginine deprivation, we starved TCR-stimulated T cells of L-arginine *in vitro*. We noted a progressive upregulation of CD98 on T cells in response to decreasing concentrations of L-arginine in the medium (Fig. 6e). Following L-arginine deprivation, T cells with the highest upregulation of CD98 showed increased expression of the transferrin receptor CD71 (Fig. 6f), suggestive of an alteration in cellular metabolism[7]. The compensatory increases in CD98 expression driven by L-arginine starvation were accompanied by substantial increases in the capacity of TCR-stimulated T cells to take up radioactively labeled phenylalanine (Fig. 6g). This was due to the specific capacity of L-arginine deprivation to increase the function of the system-L transporters utilized by essential, large, neutral amino acids such as phenylalanine and leucine, since the effect was abrogated using a small molecule inhibitor of these transporters (2-amino-2-norbornanecarboxylic acid, BCH) (Fig. 6h). Thus L-arginine starvation imposed on T cells by $arginase^+$ gMDSC has the potential to drive reprogramming of their metabolic response to TCR engagement.

Discussion

CHB is a highly prevalent disease in which the differential regulation of immune-mediated tissue damage results in markedly contrasting outcomes of infection. Using blood and liver samples from well-characterized cohorts with diverse clinical phases of acute and chronic disease, we demonstrate MDSC-mediated arginase-dependent regulation of immunopathology. A subset of MDSC with some characteristics of immature granulocytes (gMDSC) is expanded in the circulation and liver, particularly in those individuals in whom HBV replicates at high levels without triggering overt immunopathology. gMDSC potently suppress the proliferative expansion of HBV-specific and bystander T cell responses, previously implicated in the liver damage triggered by HBV infection. The correlations between circulating gMDSC, arginase I, T cell ζ-chain and the degree of liver pathology, point to the relevance of metabolic immunoregulation *in vivo*. This is further reinforced by our data showing differential expression of key amino acid transporters on virus-specific and organ-infiltrating T cells that can be driven by L-arginine starvation and modulates uptake of other essential nutrients.

Human MDSC have been shown to release arginase I upon degranulation[16], consistent with the correlation we observed between gMDSC frequencies and serum arginase I concentrations. Necrotic hepatocytes are another source of arginase I[36,37]; we previously postulated that arginase I transiently induced in acute[38] and chronic[6] flares of HBV infection might derive from damaged hepatocytes. We now show that increases in arginase I occur in the “immunotolerant” and “inactive” phases of CHB, that likely predominantly derive from the concurrent increase in arginase^{+} gMDSC, since there is minimal hepatocyte damage in these settings. The depletion of L-arginine and accompanying global T cell changes noted in the circulation[6,38,39] are unlikely to be sufficient to markedly impair peripheral immune responses, in line with the lack of obvious generalized immunosuppression. However in the local liver milieu, gMDSC accumulate, express and degranulate more arginase I, and can be visualized in close association with T cells in the narrow-lumen sinusoidal vasculature; this would maximize the effects of local nutrient depletion and any contact-dependent interactions. Activation of locally infiltrating MDSC to express more arginase I, allowing enhanced suppression of neighboring bystander T cell responses, has similarly been reported in a mouse tumor model[40].

Depriving T cells of adequate supplies of L-arginine *in vitro* inhibits their proliferation by arresting them in G0/G1[41], reflected in CD3-ζ downregulation and defects in the expansion of functional responses in CHB[6]. The capacity of gMDSC to deprive T cells of L-arginine is underscored by our new observation of a close inverse temporal correlation between gMDSC frequencies and T cell CD3-ζ chain levels *ex vivo*. We show that virus-specific T cells can also differentially regulate their expression of key amino acid transporters *in vivo*, providing an additional rheostat to modulate the intracellular availability of amino acids in persistent viral infections. This is supported by recent work demonstrating that the system-L transporter, Slc7a5, functions as a critical checkpoint to control the metabolic response of T cells to antigen[7]. We find that compensatory upregulation of system-L transporters in response to extracellular deprivation of L-arginine can enhance T cell uptake of essential amino acids like phenylalanine and leucine that, like L-arginine, regulate effector function

through mTOR[7,42]. This exemplifies a novel paradigm, whereby metabolically stressed T cells can attempt to reprogramme by selectively increasing their nutrient supply.

Although our data implicate arginase I as a major effector mechanism of the gMDSC population expanded in CHB, it is likely they can utilize supplementary suppressive mechanisms[9]. In addition to suppressing HBV-specific and bystander T cells that mediate cytolysis and produce pro-inflammatory cytokines, it remains to be determined whether MDSC can exert other anti-inflammatory effects in the HBV-infected liver. Future work should address whether gMDSC can induce Tregs to amplify their immunosuppressive effects[9], inhibit the capacity of Kupffer cells to limit immunopathology[43] or downregulate hepatic NK cells or macrophages contributing to bystander liver damage in HBV[4,5,44]. In support of this concept, work in other models has revealed inhibition of macrophage pro-inflammatory cytokines by MDSC[45] or L-arginine deprivation[46].

What factors drive and maintain the expansion of suppressive gMDSC in viral hepatitis? Our data from early acute HBV infection support a contribution for the virus in triggering their induction. Their increase in hepatotropic infections, and enrichment and enhanced function in the intrahepatic compartment, led us to question the role of the liver milieu in sustaining them. Hepatic stellate cells can promote immunosuppression by augmenting expansion of MDSC *in vitro*[29-31], as we observed, and *in vivo*[29]. The pathways involved, and whether they induce MDSC proliferation and/or enhance their survival, remain to be elucidated. In addition to the chemokine receptors we described, a number of other candidate drivers including TNF-α, IL-6, vascular endothelial growth factor, hypoxia-induced HIF-1-α[9,40,47] and γδT cells[48], merit investigation for their potential contribution to the differential accumulation of gMDSC in the distinct phases of CHB.

Our results point to a role for gMDSC in sustaining the state of immunotolerance to high levels of HBV replication characterizing the first decades of infection. The increase in gMDSC in female patients is in line with their 3–fold decreased risk of liver inflammation during CHB compared to men[17]. Patients in the immunotolerant phase of CHB, who constitute a huge infectious reservoir, have generally not been considered for antiviral therapy because of their reduced response rate and the view that their disease is immunologically inactive. However recent findings challenge this, highlighting that T cells may be less exhausted at this earlier phase of infection[49]. Our results suggest that the immunotolerant phase is characterized by active downregulation of inflammatory immune responses rather than immune ignorance, raising the possibility of targeting MDSC or amino acid metabolism to manipulate T cell responses. An important first step will be to investigate whether the expanded population of arginase^{+} gMDSC can be corrected if subjects in the immunotolerant phase are treated with existing antivirals. More broadly, our findings point to the need to investigate the role of MDSC in other types of liver disease, and serve to underscore the importance of metabolic regulation of immunopathology in the setting of chronic antigenic stimulation.

Online methods

Patients and healthy controls

This study was approved by the local ethical boards of Camden Primary Care, The Royal London Hospital, University College Hospital or The Royal Free Hospital, with all participants giving written informed consent. Donors with CHB were anti-HCV and anti-HIV antibody negative and treatment naïve, unless otherwise stated. CMV serostatus was determined by measurement of IgG using a commercial assay system (Abbot Architect). All donors with chronic HBV or HCV were stratified by serum levels of HBsAg (IU/ml) and HBeAg status (where appropriate), viral load (IU/ml, determined by real-time PCR) and degree of liver inflammation by serum alanine transaminase (ALT IU/L). Sample size was based on the standard deviation of gMDSC frequencies and the need for sufficient donors to analyse distinct disease phases. Donors with CHB were assigned to disease phases by their clinicians, who integrated virological, biochemical and histological data from several clinic visits. A cohort of 7 patients with active CHB (viral load 15,000-14million, ALT 59-1208 IU/L) were sampled on a second occasion after at least 1 year of effective antiviral therapy. Intrahepatic lymphocytes were obtained from liver biopsy material surplus to diagnostic requirements; liver necroinflammation was scored as part of their routine histological assessment using the Knodell score for Histological Activity Index. Characteristics of all patients and controls are summarised in Supplementary Table I.

PBMC and intrahepatic lymphocyte isolation

PBMC were isolated by gradient centrifugation on Ficoll-Hypaque Plus (GE Healthcare) and used immediately as described below. Sera were collected and frozen for later use. Intrahepatic lymphocytes were isolated as previously described [6].

Assessment of absolute number of gMDSC

Absolute counts for gMDSC were assessed using BD TruCount tubes from heparinised whole blood on a small cohort of healthy controls and subjects with CHB according to the manufacturer's instructions (BD Bioscience).

Flow cytometric analysis

Multi-parametric flow cytometry was used for phenotypic and functional analysis of PBMC. For gMDSC phenotyping, combinations of the following monoclonal antibodies (mAb) were used: CD11b-PECy7, HLA-DR-eFluor450, CD33-AlexaFluor700, CD16-APC-eFluor780, CD63-PE, CD15-APC, CD14-HorizonV500, CD66b-PerCPCy5.5, CXCR1-FITC, CCR2-PE, CXCR3-PerCPCy5.5, CXCR4-PE, MPO-PE and arginase I-FITC. For T cell analysis, combinations of the following mAb were used: CD3ε-PECy7, CD8-AlexaFluor700, CD4-APC-eFluor780, CD3-ζ-PE, granzyme B-FITC, HLA-DR-HorizonV500, CD14-HorizonV500, CD19-BD-HorizonV500, IFN-γ-HorizonV450, Ki67-PE, TNF-α-APC, CD98-FITC and CD71-APCCy7. Full details can be found in Supplementary Table 2. Briefly, cells were stained with a fixable Live/Dead dye (Life Technologies) before being stained for surface mAb; 30 minutes at 4 °C with saturating concentrations of mAb in the presence of FcR blocking reagent (Miltenyi Biotec). Cells

were fixed and permeablized with Cytofix/Cytoperm (BD Bioscience) and intracellular proteins detected with saturating mAb; 30 minutes at 4 °C. All samples were acquired on a LSRII (BD Biosciences) and analyzed using FlowJo (Tree Star).

Dextramer staining of virus-specific T cells

HBV- and CMV-specific HLA-A2 dextramers (Immudex) were used for detection of virus-specific cells. For detection of HBV-specific $CD8^+$ T cells the following pool of HLA-A2/peptide dextramers was used: core 18-27 (FLPSDFFPSV), envelope 183-91 (FLLTRILTI), envelope 335-42 (WLSLLVPFV), envelope 348-57 (GLSPTVWLSV), polymerase 455-463 (GLSRYVARL), polymerase 502-10 (KLHLYSHPI) and for CMV-specific T cell detection a dextramer against the HLA-A2-restricted CMV epitope: NLVPMVATV was used. As a control for non-specific dextramer binding, a dextramer loaded with an irrelevant peptide was used in parallel. Briefly, cells were stained with dextramers; 37 °C in PBS, washed twice in cRPMI and left to rest for 1hr before further mAb staining as above. During analysis, stringent gating criteria were applied with doublet, dead cell and $CD19^+$, $CD14^+$ exclusion to minimize non-specific binding contamination.

Detection of serum arginase-1

Arginase I was detected in sera from healthy controls and subjects with CHB by ELISA, according to the manufacturer's instructions (Hycult).

Tandem HPLC-MS for amino acid quantification

Circulating L-arginine, L-tryptophan and L-phenylalanine levels were determined from sera using tandem high-performance liquid chromatography with mass spectrometry detection (tandem HPLC-MS), with the stable isotope dilution method. Briefly, a known concentration of a stable isotope-labeled amino acid (Cambridge Isotopes) was added to sera for later determination of recovery. Sera were then de-proteinised by the addition of cold trichloroacetic acid (TCA, Fisher) and samples centrifuged (13,000 rpm, 10 minutes, 4 °C) to remove bulk protein. The supernatant was separated using a Dionex Ultimate 3000 HPLC system (Dionex) fitted with a Pinnacle DB biphenyl column (1.9 μm, 50×21 mm; Thames Restek) at a flow rate of 0.4 ml/min using a gradient mobile phase of water:acetonitrile with 0.1% formic acid (10% acetonitrile rising to 90% over 6 minutes) and measured using a Orbitrap XL (Thermo Fisher) mass spectrometer in positive ion mode. Sample concentrations were determined by comparison to standard curves and corrected for recovery using the added stable isotopes.

gMDSC Suppression Assays

gMDSC were enriched or depleted using sequential magentic bead isolation: CD14 and CD15 positive selection kits ($CD14^-CD15^+$) (Miltenyi Biotec) as per the manufacturer's instructions. In selected cases gMDSC were highly purified by flow cytometry on the basis of CD11b, CD14 and CD15 expression on a FACSAria (BD Bioscience). Where indicated PBMC or PBMC enriched/depleted of gMDSC were stimulated with either: 0.5 μg/ml of an HLA-A and HLA-B-restricted peptide pool spanning the immune-dominant proteins of CMV, EBV and influenza (CEF) (JPT Peptide Technologies), 1 μg/ml overlapping peptides

(pool of 15-mer peptides overlapping by 10 residues) spanning the core of HBV genotype D (JPT Peptide Technologies), 1 μg/ml HLA-A2-restricted NLVPMVATV peptide from CMV pp65 (ProImmune) or 0.5 μg/ml plate-bound anti-CD3 and 0.5 μg/ml anti-CD28 (eBioscience). All cultures were carried out in the presence of 20 IU/ml recombinant human IL-2 (Miltenyi Biotec) in cRPMI (Life Technologies) for 5-7 days at 37 °C. Specific responses were detected by intracellular cytokine staining after re-stimulation on day 4/6 in the presence of 1 μg/ml brefeldin-A (BFA, Sigma-Aldrich). Where indicated, 0.5 mM *N*-hydroxyl-nor-L-arginine (nor-NOHA) (Calbiochem), an arginase I specific inhibitor, was added to the culture on day 0.

Specific enzymatic activity of arginase I

Human liver tissue was homogenised (TissueLyser II, Qiagen) in ice-cold Tris-HCL buffer (10mM, pH 7.2; with 158 mM NaCl, 1 mM EDTA and 1% Triton ×100) at a ratio of 1:4 tissue to buffer. Isolates were then centrifuged (13,000 rpm at 4 °C for 10 minutes) to remove the remaining solid material. For the determination of arginase I activity, supernatant from the tissue preparation was incubated at increasing pH to determine the rate of conversion of L-arginine to urea. To start the reaction, tissue supernatant (100 μl) was added to a solution containing $MnCl_2$ (0.7 mM), Saponin (0.3%) and L-arginine (18 mM) in glycine-NaOH buffer (50 mM) at pH values of 7.5, 8, 8.5, 9 and 9.5. The solutions were incubated at 37 °C, with aliquots removed at time 0, 20 and 40 minutes. The reaction stopped by the addition of tungstic acid solution (2.5% w/v, in 1 M HCL, 1 M H_2SO_4) at a ratio of 3:1 reaction mix:stop solution. Urea concentrations were determined in the resulting supernatant using a COBAS Integra II clinical analyzer (Roche) according to manufacturers instructions. Enzyme activity was calculated in IU as μmoles urea produced per minute per gram of wet weight tissue.

Imagestream Analysis

ImageStream technology was used to analyze the intracellular distribution of arginase I. PBMC were isolated and stained using the following mAb: CD11b-PEcy7, CD15-AlexaFluor700, CD16-PE, HLA-DR-V500, arginase I-FITC. After staining, cells were fixed using Cytofix/Cytoperm (BD Bioscience) as per the manufacturer's protocol. The sample was processed on an Amnis ImageStreamX Imaging Flow Cytometer (MERK-Millipore) fitted with a 60× microscope objective. Raw image files were acquired using INSPIRE software. After acquisition, a compensation matrix was applied to the data to correct for spectral overlap. Data analysis was done using IDEAS software, displaying PBMC using gradient RMS for the brightfield channel to exclude out of focus cells and a combined Area to Aspect Ratio dot plot ensured gating on single-cell events. Cells were then gated as: $CD11b^+CD15^+CD16^+$ for gMDSC identification, excluding cells expressing HLA-DR.

Primary hepatic stellate cell isolation

Primary hepatic stellate cells (pHSC) were isolated from normal liver margins in patients undergoing hepatic resection for metastatic cancer. All patients signed informed consent, approved by the Royal Free Hospital ethics committee. For extraction of pHSC, fresh post-resection liver tissue was washed thoroughly, passed through a tissue press and digested

with DNAseI (0.001%, Roche) and collagenase IV (0.01%, Life Technologies). Cellular homogenate was filtered through a 70 μm cell strainer and centrifuged at low speed to remove remaining parenchymal cells, then at 450 g to wash the cells. The remaining cells were layered for density gradient isolation using Optiprep (Sigma-Aldrich). After isolation, pHSC were suspended in Stellate Cell Medium® (ScienCell Research Laboratories), plated at a density of 5×10^4 cells/cm in tissue culture flasks and cultured at 37 °C in a humidified atmosphere with 5% CO_2. On day 2-4, cell debris and non-adherent cells were removed by washing. When cultures reached confluence, cells were trypsinized and replated; cells were passaged twice before freezing.

Primary hepatic stellate co-culture

Pre-isolated pHSC were thawed and cultured in 25 cm^2 tissue culture flasks in Stellate Cell Medium® to approximately 90% confluence. Cells were detached with trypsin–EDTA (Life Technologies), re-plated in 24 well plates in cRPMI with 10% FBS at 50,000 cells/well and left for 24–48 hrs to adhere. Once plated pHSC were incubated with 2×10^6 freshly isolated PBMC in cRPMI for 6 days prior to staining for gMDSC frequencies as above.

CD98 upregulation upon amino acid starvation

To assess the upregulation of amino acid transporters on the surface of T cells, whole PBMC were stimulated with 0.5 μg/ml plate bound anti-CD3 for 3 days in cRPMI in flat bottom 96 well plates. On day 3 PBMC were transferred to U bottom 96 well plates, washed once in PBS, and replaced for 24 hrs with: RPMI, L-arginine free media, or RPMI supplemented with 50 μM L-arginine, all without FBS. After culture PBMC were stained for live/dead, CD3, CD98 and CD71 as above.

Amino acid uptake

Between 0.5 and 1×10^6 cells were resuspended in 0.4 ml Hank's balanced-salt solution (Life Technologies) containing ^{3H}L-phenylalanine (0.5 μCi/ml) (Perkin Elmer) with a final extracellular L-leucine concentration of 5 μM. Where indicated, 10 mM BCH (2-aminobicyclo-(2,2,1)-heptane-2-carboxylic acid, Sigma) was added to the uptake medium. Amino acid uptake was assayed for 4 minutes with samples layered over 0.5 ml of a mixture of silicone oil (Dow Corning 550 (BDH silicone products); specific density, 1.07 g/ml) and dibutyl phthalate (Fluka) at a ratio of 1:1. Cells were pelleted below the oil, the uptake media above the oil layer aspirated. Following 3 washes, the silicon oil–dibutyl phthalate mixture was aspirated, and the cell pellet underneath was resuspended in 200 μl NaOH (500 mM). β-radioactivity was measured by liquid scintillation counting in a Beckman LS 6500 Multi-Purpose Scintillation Counter (Beckman Coulter). Each data point was performed in triplicate.

Immunohistochemistry

Core needle biopsy specimens were obtained from patients with CHB for diagnostic purposes and were formalin-fixed and paraffin-embedded. Immunohistochemistry was carried out using a Leica BondMax immunostainer (Leica Biosystems, UK). Slides were de-waxed, rehydrated, subjected to heat-induced epitope retrieval (HIER) using sodium citrate

buffer, pH 6, or EDTA-TRIS buffer, pH 9, for 10 minutes, and allowed to cool, followed by 15 minutes incubation at room temperature with the primary antibody (CD15 (Rabbit) – Novus Biologicals NBP2-21754 1:50 pH 6, CD66b (Mouse) – BD Biosciences 555723 1:50 pH 9, CD3 (Rabbit) – Dako A0452 1:100 pH 9). The signal was detected using the Leica Polymer Refine Detection System, Rabbit/Mouse (DAB) and Leica Polymer Define Red Detection System, Rabbit/Mouse (Fast Red), catalogue numbers DS9800 and DS9390. The slides were then dehydrated with alcohol, cleared with xylene and cover slipped with DPX (Leica Biosystems, UK) after hematoxylin counterstaining. Images were captured and processed with a Nikon Eclipse E600 microscope using the Nuance™ 3.0.2 (PerkinElmer, UK) multispectral imaging technology. Distinguishing between brown and red and unmixing these co-localized chromogens was not feasible by eye or with an RGB camera so a multispectral approach was used. Nuance camera takes several images over different wavelengths, thus identifying the 'individual spectral signature' of each chromogen, saving and unmixing it from adjacent colours. Once unmixed, the images were re-coloured, enabling distinction of chromogens and inverting to a pseudo-fluorescence image.

Statistical analysis

Natural variance in the data is demonstrated, as all data are displayed for cohort analysis. Statistical analyses were performed in Prism (GraphPad) using appropriate tests as indicated in legends (unpaired *t* test, paired *t* test, one way ANOVA (Tukeys multiple comparisons test), or Pearson product-moment correlation coefficient), with significant differences marked on all figures. All test were carried out as two-tail tests and for all tests, significance levels were defined as: * = $p<0.05$, ** = $p<0.005$, *** = $p<0.001$. Multivariate analyses were conducted in R 3.0.2, an open-source programming language for statistical computing. Hierarchical clustering was performed using Euclidean distance as the metric to calculate the similarity of each subject to one another.

Supplementary Material

Refer to Web version on PubMed Central for supplementary material.

Acknowledgements

This work was funded by UK Medical Research Council grant G0801213 to MKM, UK Medical Research Council studentship to LJP, Medical Research Council / AStar grant G0901374 to MKM and AB, Wellcome Trust Senior Investigator Award to MKM, National Health and Medical Research Council Postgraduate Research Scholarship to KPS. We thank Pascale Kropf for advice on the assessment of gMDSC arginase I release, Richard Milne, Eleni Nastouli and the Clinical Virology Departments at University College Hospital and the Royal Free Hospital for CMV serology and HBsAg quantification, Oltin Pop and Chris Starling for assistance with immunostaining. We are very grateful to all patients and control volunteers who participated in this study and to clinical staff who helped with participant recruitment and monitoring.

References

1. Guidotti LG, Chisari FV. Immunobiology and pathogenesis of viral hepatitis. Annu Rev Pathol. 2006; 1:23–61. [PubMed: 18039107]
2. Maini MK, et al. The role of virus-specific CD8(+) cells in liver damage and viral control during persistent hepatitis B virus infection. J Exp Med. 2000; 191:1269–1280. [PubMed: 10770795]

3. Bertoletti A, Maini MK. Protection or damage: a dual role for the virus-specific cytotoxic T lymphocyte response in hepatitis B and C infection? Curr Opin Immunol. 2000; 12:403–408. [PubMed: 10899021]
4. Kakimi K, et al. Blocking chemokine responsive to gamma-2/interferon (IFN)-gamma inducible protein and monokine induced by IFN-gamma activity in vivo reduces the pathogenetic but not the antiviral potential of hepatitis B virus-specific cytotoxic T lymphocytes. J Exp Med. 2001; 194:1755–1766. [PubMed: 11748277]
5. Sitia G, et al. MMPs are required for recruitment of antigen-nonspecific mononuclear cells into the liver by CTLs. J Clin Invest. 2004; 113:1158–1167. [PubMed: 15085195]
6. Das A, et al. Functional skewing of the global CD8 T cell population in chronic hepatitis B virus infection. J Exp Med. 2008; 205:2111–2124. [PubMed: 18695005]
7. Sinclair LV, et al. Control of amino-acid transport by antigen receptors coordinates the metabolic reprogramming essential for T cell differentiation. Nat Immunol. 2013; 14:500–508. [PubMed: 23525088]
8. Pearce EL, Poffenberger MC, Chang CH, Jones RG. Fueling immunity: insights into metabolism and lymphocyte function. Science. 2013; 342:1242454. [PubMed: 24115444]
9. Gabrilovich DI, Ostrand-Rosenberg S, Bronte V. Coordinated regulation of myeloid cells by tumours. Nat Rev Immunol. 2012; 12:253–268. [PubMed: 22437938]
10. Norris BA, et al. Chronic but not acute virus infection induces sustained expansion of myeloid suppressor cell numbers that inhibit viral-specific T cell immunity. Immunity. 2013; 38:309–321. [PubMed: 23438822]
11. Qin A, et al. Expansion of monocytic myeloid-derived suppressor cells dampens T cell function in HIV-1-seropositive individuals. J Virol. 2013; 87:1477–1490. [PubMed: 23152536]
12. Tacke RS, et al. Myeloid suppressor cells induced by hepatitis C virus suppress T-cell responses through the production of reactive oxygen species. Hepatology. 2012; 55:343–353. [PubMed: 21953144]
13. Vollbrecht T, et al. Chronic progressive HIV-1 infection is associated with elevated levels of myeloid-derived suppressor cells. AIDS. 2012; 26:F31–37. [PubMed: 22526518]
14. Kotsakis A, et al. Myeloid-derived suppressor cell measurements in fresh and cryopreserved blood samples. J Immunol Methods. 2012; 381:14–22. [PubMed: 22522114]
15. Brandau S, Moses K, Lang S. The kinship of neutrophils and granulocytic myeloid-derived suppressor cells in cancer: cousins, siblings or twins? Semin Cancer Biol. 2013; 23:171–182. [PubMed: 23459190]
16. Rodriguez PC, et al. Arginase I-producing myeloid-derived suppressor cells in renal cell carcinoma are a subpopulation of activated granulocytes. Cancer research. 2009; 69:1553–1560. [PubMed: 19201693]
17. Chu CM, Sheen IS, Lin SM, Liaw YF. Sex difference in chronic hepatitis B virus infection: studies of serum HBeAg and alanine aminotransferase levels in 10,431 asymptomatic Chinese HBsAg carriers. Clinical infectious diseases: an official publication of the Infectious Diseases Society of America. 1993; 16:709–713. [PubMed: 8507764]
18. Cloke T, Munder M, Taylor G, Muller I, Kropf P. Characterization of a novel population of low-density granulocytes associated with disease severity in HIV-1 infection. PloS one. 2012; 7:e48939. [PubMed: 23152825]
19. Munder M, et al. Arginase I is constitutively expressed in human granulocytes and participates in fungicidal activity. Blood. 2005; 105:2549–2556. [PubMed: 15546957]
20. Frumento G, et al. Tryptophan-derived catabolites are responsible for inhibition of T and natural killer cell proliferation induced by indoleamine 2,3-dioxygenase. J Exp Med. 2002; 196:459–468. [PubMed: 12186838]
21. Folley SJ, Greenbaum AL. Determination of the arginase activities of homogenates of liver and mammary gland: effects of pH and substrate concentration and especially of activation by divalent metal ions. The Biochemical journal. 1948; 43:537–549. [PubMed: 16748448]
22. Ikemoto M, et al. A useful ELISA system for human liver-type arginase, and its utility in diagnosis of liver diseases. Clinical biochemistry. 2001; 34:455–461. [PubMed: 11676974]

23. van de Poll MC, et al. Elevated plasma arginase-1 does not affect plasma arginine in patients undergoing liver resection. Clin Sci (Lond). 2008; 114:231–241. [PubMed: 17708746]
24. Rotondo R, et al. Exocytosis of azurophil and arginase 1-containing granules by activated polymorphonuclear neutrophils is required to inhibit T lymphocyte proliferation. J Leukoc Biol. 2011; 89:721–727. [PubMed: 21330347]
25. Talmadge JE, Gabrilovich DI. History of myeloid-derived suppressor cells. Nature reviews. Cancer. 2013; 13:739–752.
26. Eash KJ, Means JM, White DW, Link DC. CXCR4 is a key regulator of neutrophil release from the bone marrow under basal and stress granulopoiesis conditions. Blood. 2009; 113:4711–4719. [PubMed: 19264920]
27. Ma Q, Jones D, Springer TA. The chemokine receptor CXCR4 is required for the retention of B lineage and granulocytic precursors within the bone marrow microenvironment. Immunity. 1999; 10:463–471. [PubMed: 10229189]
28. Friedman SL. Hepatic stellate cells: protean, multifunctional, and enigmatic cells of the liver. Physiological reviews. 2008; 88:125–172. [PubMed: 18195085]
29. Chou HS, et al. Hepatic stellate cells regulate immune response by way of induction of myeloid suppressor cells in mice. Hepatology. 2011; 53:1007–1019. [PubMed: 21374665]
30. Hochst B, et al. Activated human hepatic stellate cells induce myeloid derived suppressor cells from peripheral blood monocytes in a CD44-dependent fashion. Journal of hepatology. 2013; 59:528–535. [PubMed: 23665041]
31. Zhao W, et al. Hepatic stellate cells promote tumor progression by enhancement of immunosuppressive cells in an orthotopic liver tumor mouse model. Laboratory investigation; a journal of technical methods and pathology. 2014; 94:182–191.
32. Rodriguez PC, et al. Regulation of T cell receptor CD3zeta chain expression by L-arginine. J Biol Chem. 2002; 277:21123–21129. [PubMed: 11950832]
33. Hayashi K, Jutabha P, Endou H, Sagara H, Anzai N. LAT1 is a critical transporter of essential amino acids for immune reactions in activated human T cells. J Immunol. 2013; 191:4080–4085. [PubMed: 24038088]
34. Cantor JM, Ginsberg MH. CD98 at the crossroads of adaptive immunity and cancer. Journal of cell science. 2012; 125:1373–1382. [PubMed: 22499670]
35. Campbell WA, et al. TA1/LAT-1/CD98 light chain and system L activity, but not 4F2/CD98 heavy chain, respond to arginine availability in rat hepatic cells. Loss Of response in tumor cells. The Journal of biological chemistry. 2000; 275:5347–5354. [PubMed: 10681508]
36. Schumacher K, Maerker-Alzer G, Wehmer U. A lymphocyte-inhibiting factor isolated from normal human liver. Nature. 1974; 251:655–656. [PubMed: 4422189]
37. Chisari FV, et al. Production of two distinct and independent hepatic immunoregulatory molecules by the perfused rat liver. Hepatology. 1985; 5:735–743. [PubMed: 3928477]
38. Sandalova E, et al. Increased levels of arginase in patients with acute hepatitis B suppress antiviral T cells. Gastroenterology. 2012; 143:78–87. e73. [PubMed: 22475535]
39. Walker LJ, et al. CD8alphaalpha Expression Marks Terminally Differentiated Human CD8+ T Cells Expanded in Chronic Viral Infection. Front Immunol. 2013; 4:223. [PubMed: 23964274]
40. Corzo CA, et al. HIF-1alpha regulates function and differentiation of myeloid-derived suppressor cells in the tumor microenvironment. The Journal of experimental medicine. 2010; 207:2439–2453. [PubMed: 20876310]
41. Rodriguez PC, Quiceno DG, Ochoa AC. L-arginine availability regulates T-lymphocyte cell-cycle progression. Blood. 2007; 109:1568–1573. [PubMed: 17023580]
42. Hara K, et al. Amino acid sufficiency and mTOR regulate p70 S6 kinase and eIF-4E BP1 through a common effector mechanism. The Journal of biological chemistry. 1998; 273:14484–14494. [PubMed: 9603962]
43. Sitia G, et al. Kupffer cells hasten resolution of liver immunopathology in mouse models of viral hepatitis. PLoS pathogens. 2011; 7:e1002061. [PubMed: 21655107]
44. Dunn C, et al. Cytokines induced during chronic hepatitis B virus infection promote a pathway for NK cell-mediated liver damage. J Exp Med. 2007; 204:667–680. [PubMed: 17353365]

45. Sander LE, et al. Hepatic acute-phase proteins control innate immune responses during infection by promoting myeloid-derived suppressor cell function. The Journal of experimental medicine. 2010; 207:1453–1464. [PubMed: 20530204]
46. Mieulet V, et al. TPL-2-mediated activation of MAPK downstream of TLR4 signaling is coupled to arginine availability. Science signaling. 2010; 3:ra61. [PubMed: 20716763]
47. Sade-Feldman M, et al. Tumor necrosis factor-alpha blocks differentiation and enhances suppressive activity of immature myeloid cells during chronic inflammation. Immunity. 2013; 38:541–554. [PubMed: 23477736]
48. Kong X, Sun R, Chen Y, Wei H, Tian Z. gammadeltaT cells drive myeloid-derived suppressor cell-mediated CD8+ T cell exhaustion in hepatitis B virus-induced immunotolerance. J Immunol. 2014; 193:1645–1653. [PubMed: 25015833]
49. Kennedy PT, et al. Preserved T-cell function in children and young adults with immune-tolerant chronic hepatitis B. Gastroenterology. 2012; 143:637–645. [PubMed: 22710188]

Europe PMC Funders Author Manuscripts

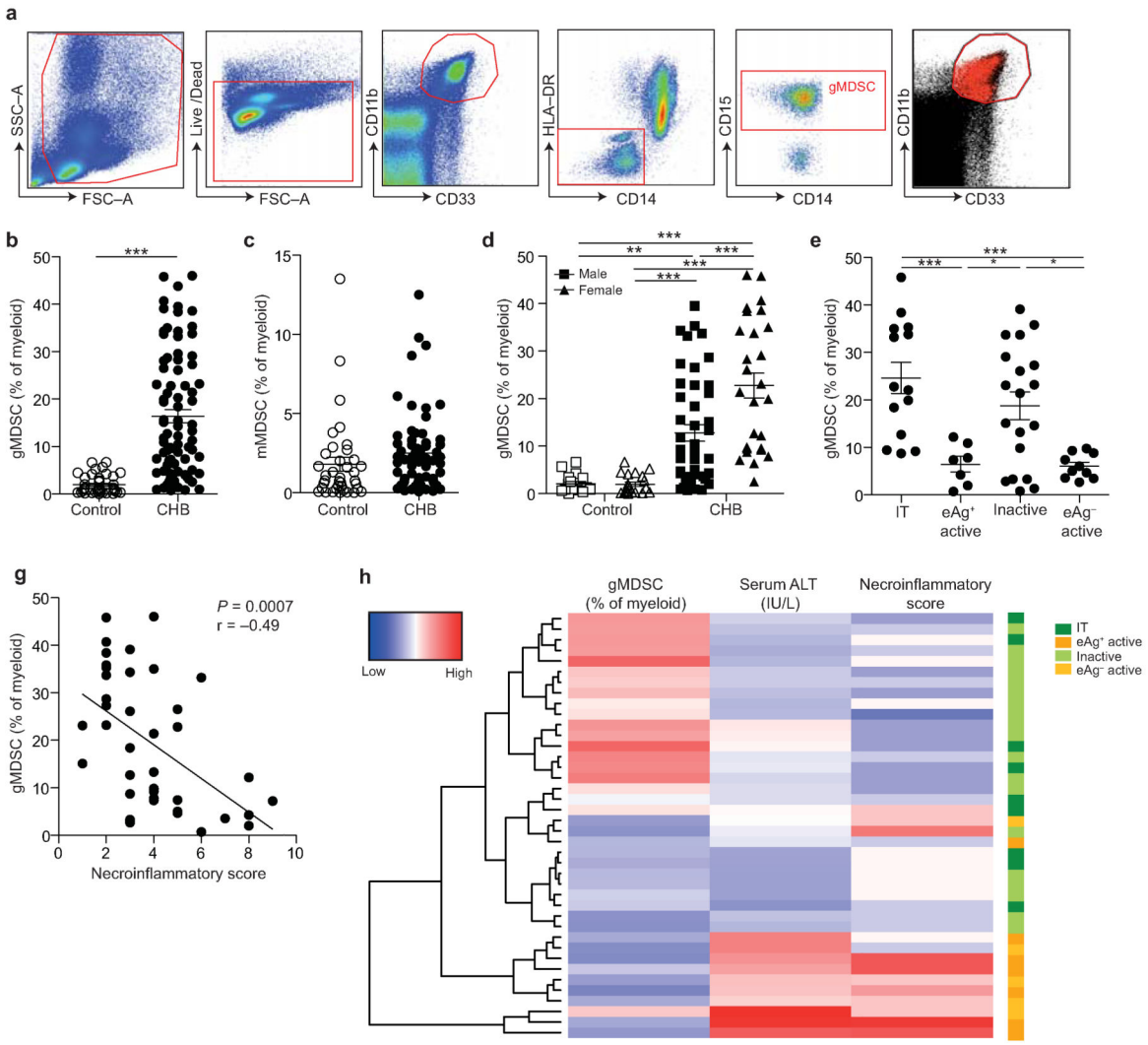

Figure 1. gMDSC expand in subjects replicating HBV in the absence of immunopathology

a) Sequential gating strategy for gMDSC identification ($CD11b^{high}CD33^{+}HLA\text{-}DR^{-}CD14^{-}CD15^{+}$) using 11-color flow cytometry from freshly isolated PBMC (doublet discrimination not shown). gMDSC population (superimposed in red) was calculated as a percentage of myeloid cells ($CD11b^{high}CD33^{+}$). Cumulative dot plots showing circulating **b**) gMDSC and **c**) mMDSC frequencies (n=44, healthy controls; n=84, CHB). **d**) gMDSC frequencies analyzed by gender. **e**) Summary plot of frequencies classified by disease phase using a subset of the cohort with clearly defined disease phases: 14 “immunotolerants” ($HBeAg^{+}$, HBV DNA $>10^{7}$ IU/ml, ALT <40 IU/L), 9 “eAg^{+} active disease” (HBV DNA $>5\times10^{5}$ IU/ml, ALT >60 IU/L), 21 “inactive disease” ($HBeAg^{-}$, HBV DNA <2000 IU/ml, ALT <40 IU/L), 11 “eAg^{-} active disease” ($HBeAg^{-}$, HBV DNA $>5\times10^{5}$ IU/ml, ALT >60 IU/L). **f**) gMDSC frequencies according to hepatic necroinflammatory score (n=42, CHB). **g**) Unsupervised hierarchical clustering using Euclidean distance; dendrogram displaying similarity between clusters. Clinically assigned disease phase, shown adjacent to plot; immunotolerant: dark green, eAg^{+} active disease: dark yellow, inactive disease: pale green, eAg^{-} active disease: pale yellow (not used for analysis). Increasing color intensity (blue–

red) corresponds to increasing gMDSC frequency, ALT (IU/L) or necroinflammatory score (n=42, CHB; maximum Knodell score in this cohort = 9/18). Error bars represent the mean ± SEM for the cohorts indicated; * $p<0.05$, ** $p<0.01$; *** $p<0.001$; **b-c** unpaired *t* test; **d-e** one way ANOVA (Tukey's multiple comparisons test); **f** Pearson product-moment correlation coefficient.

Europe PMC Funders Author Manuscripts

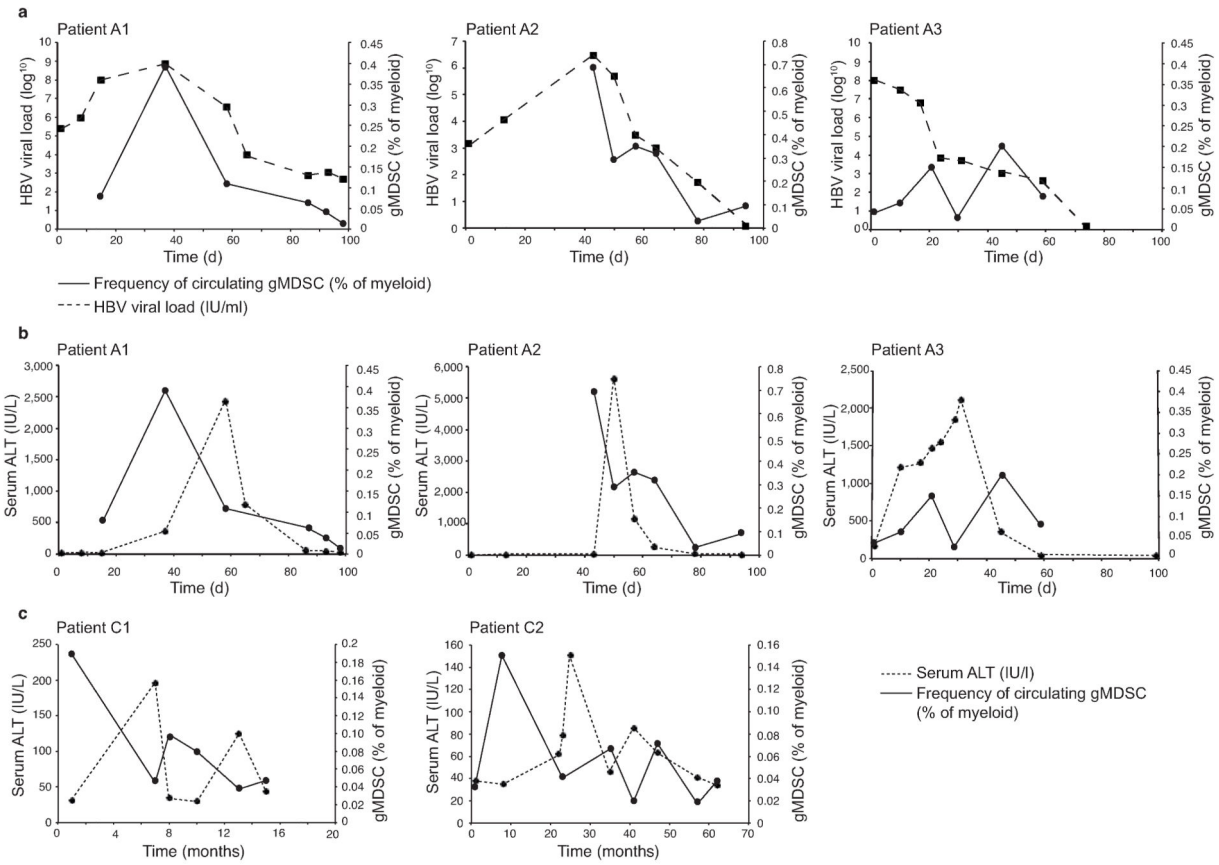

Figure 2. gMDSC are transiently induced in acute HBV infection and decline before acute and chronic hepatic flares

gMDSC were quantitated as a percentage of total myeloid cells ($CD11b^{high}CD33^{+}$) from PBMC cryopreserved from multiple time points from the onset of viraemia and subsequent hepatic flare. **a**) gMDSC frequencies in relation to viral load in three subjects with acute HBV infection sampled from the pre-clinical phase through to HBV disease resolution. **b**) gMDSC frequencies plotted with the temporal course of liver inflammation (serum ALT, IU/L) in the same three patients with acute HBV and **c**) in two subjects experiencing spontaneous flares of chronic $HBeAg^{-}$ disease (days or months from initial presentation in clinic).

Europe PMC Funders Author Manuscripts

Europe PMC Funders Author Manuscripts

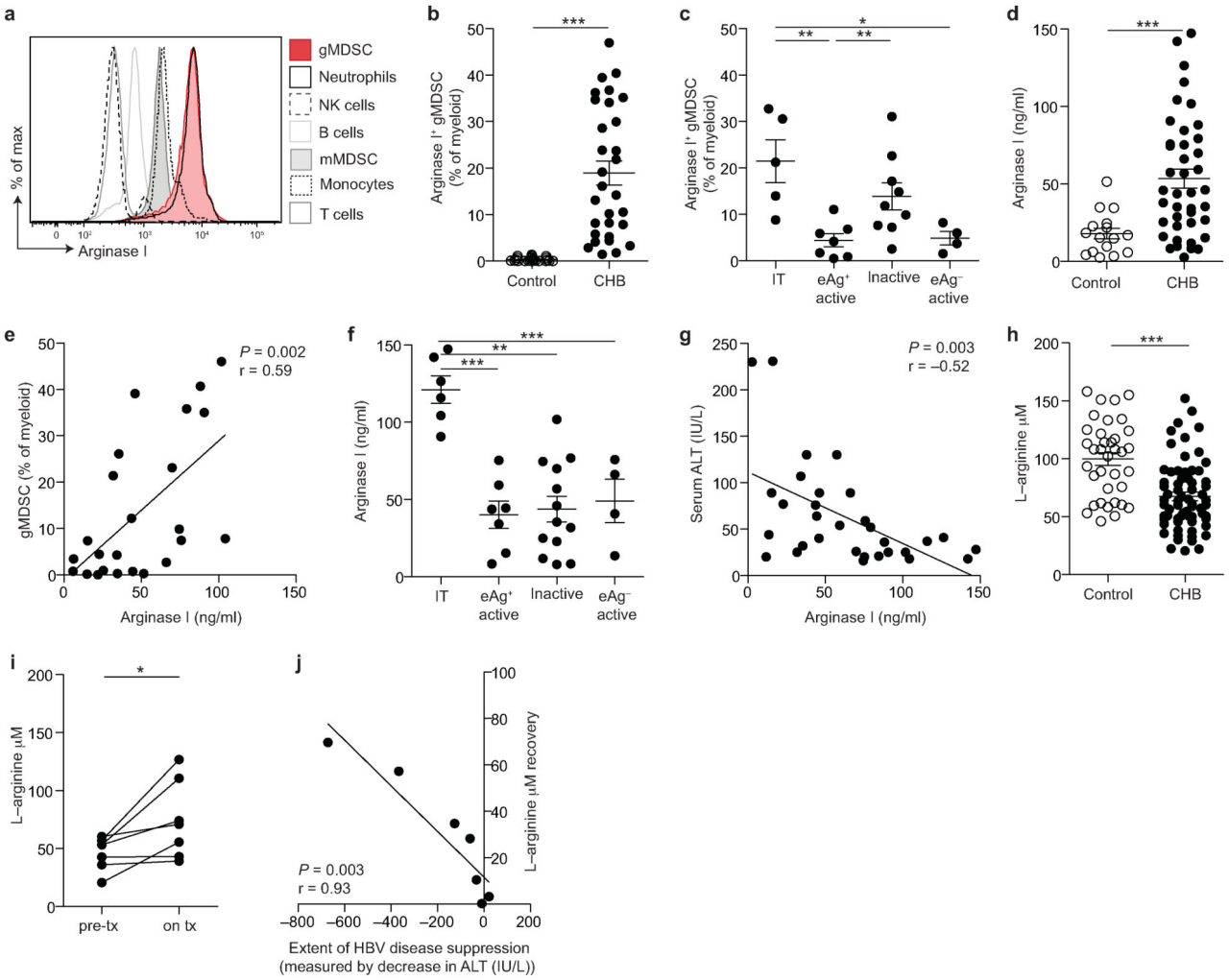

Figure 3. Arginase^{+} gMDSC and circulating arginase I increase in patients with HBV replication without immunopathology, whilst L-arginine levels decline

a) Analysis of PBMC subpopulations for expression (MFI) of intracellular arginase I. Cellular fractions identified as: CD3^{-}CD19^{+} B cells, CD14^{-} CD16^{+}CD15^{+} low density neutrophils, CD3^{+} T cells, CD3^{-}CD56^{+} NK cells, HLA-DR^{+}CD14^{+} monocytes, CD11b^{high}CD33^{+}HLA-DR^{low}CD14^{+}CD15^{-} mMDSC. **b**) Cumulative data for percentage of arginase-I-expressing gMDSC as a proportion of total myeloid cells (CD11b^{high}CD33^{+}; n=25, healthy controls; n=31, CHB). **c**) Arginase^{+} gMDSC as a percentage of total myeloid cells categorised by disease phase (defined in the legend to Figure 1). **d**) Serum arginase I (ng/ml) concentration, determined by ELISA (n=16, healthy controls; n=41, CHB). **e**) Correlation of serum arginase I with circulating gMDSC frequencies (n=24, CHB). Further cumulative analysis of the CHB cohort by: **f**) disease phase, **g**) serum ALT (IU/L). **h**) Tandem high-performance liquid chromatography mass spectrometry analysis of the L-arginine concentration (µM) in sera (n=38, healthy controls; n=71, CHB). **i**) L-arginine concentration (µM) in sera from 7 CHB pre– and on antiviral therapy (for >1 year) and **j**) correlation between decline in liver inflammation on therapy (ALT, IU/L) and recovery of L-arginine levels. Error bars represent the mean ± SEM for the cohorts indicated; * p<0.05,

** p<0.01; *** p<0.001; **b, d, h** unpaired *t* test, **i** paired *t* test, **e, g, j** Pearson product-moment correlation coefficient; **c, f** one way ANOVA (Tukey's multiple comparisons test).

Europe PMC Funders Author Manuscripts

Europe PMC Funders Author Manuscripts

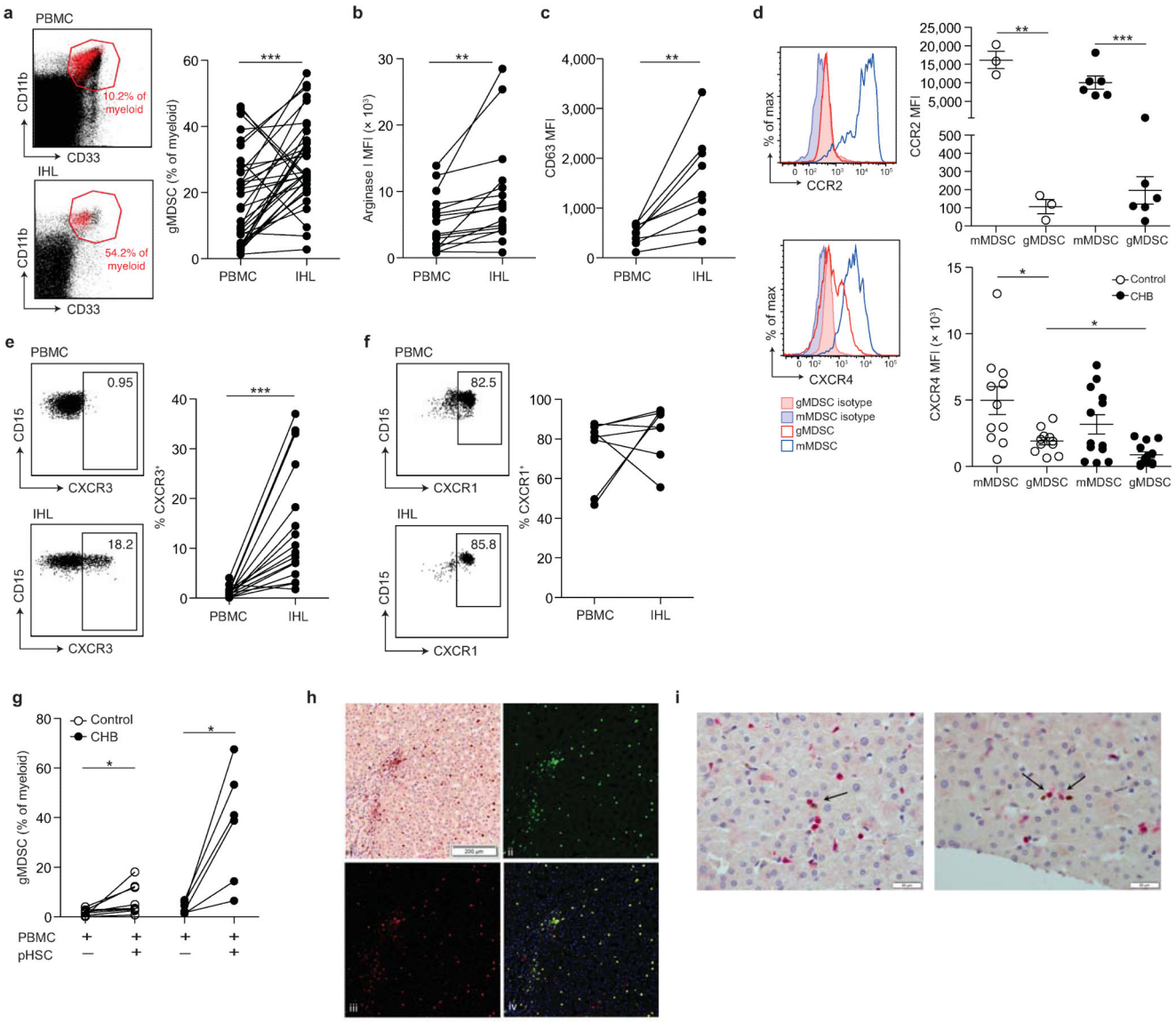

Figure 4. Accumulation of arginase^{+} gMDSC in the liver

a) Representative FACS plots showing gMDSC (red) superimposed on the immature myeloid cell population from paired PBMC and intrahepatic leukocyte (IHL) samples, and the cumulative data depicting circulating compared to intrahepatic gMDSC frequencies (n=36, CHB). **b**) Cumulative data depicting expression (MFI) of arginase I in circulating and intrahepatic gMDSC (n=16, CHB). **c**) Surface CD63 expression (MFI) on peripheral and intrahepatic gMDSC (n=9, CHB). **d**) Representative and cumulative chemokine receptor expression on mMDSC and gMDSC of CCR2 and CXCR4. Representative and cumulative expression (%) on paired peripheral and intrahepatic gMDSC of **e**) CXCR3 (n=16, CHB) and **f**) CXCR1 (n=8, CHB). **g**) PBMC co-cultured with or without pHSC and analysed for gMDSC frequencies on day 6 (n=9, healthy controls, n=8, CHB). **h**) Representative double epitope immunostaining of liver sections from subjects with CHB for CD15 (brown, DAB) and CD66b (red, APAAP) at 100× magnification (top left); multispectral analysis (Nuance)

with CD15 (green, top right) and CD66b (red, bottom left) as pseudo-fluorescent images. Co-localization of CD15 and CD66b, represented in yellow; composite image (bottom right). **i**) Two representative examples of double epitope immunohistochemistry with CD3 in red (APAAP) and CD66b in brown (DAB) at 400× magnification: arrows indicate $CD3^+$ and $CD66b^+$ cells in close association. Error bars represent the mean ± SEM for the cohorts indicated; * $p<0.05$; ** $p<0.01$; *** $p<0.001$; **a-c, e-g** paired *t* test; **d** unpaired *t* test.

Europe PMC Funders Author Manuscripts

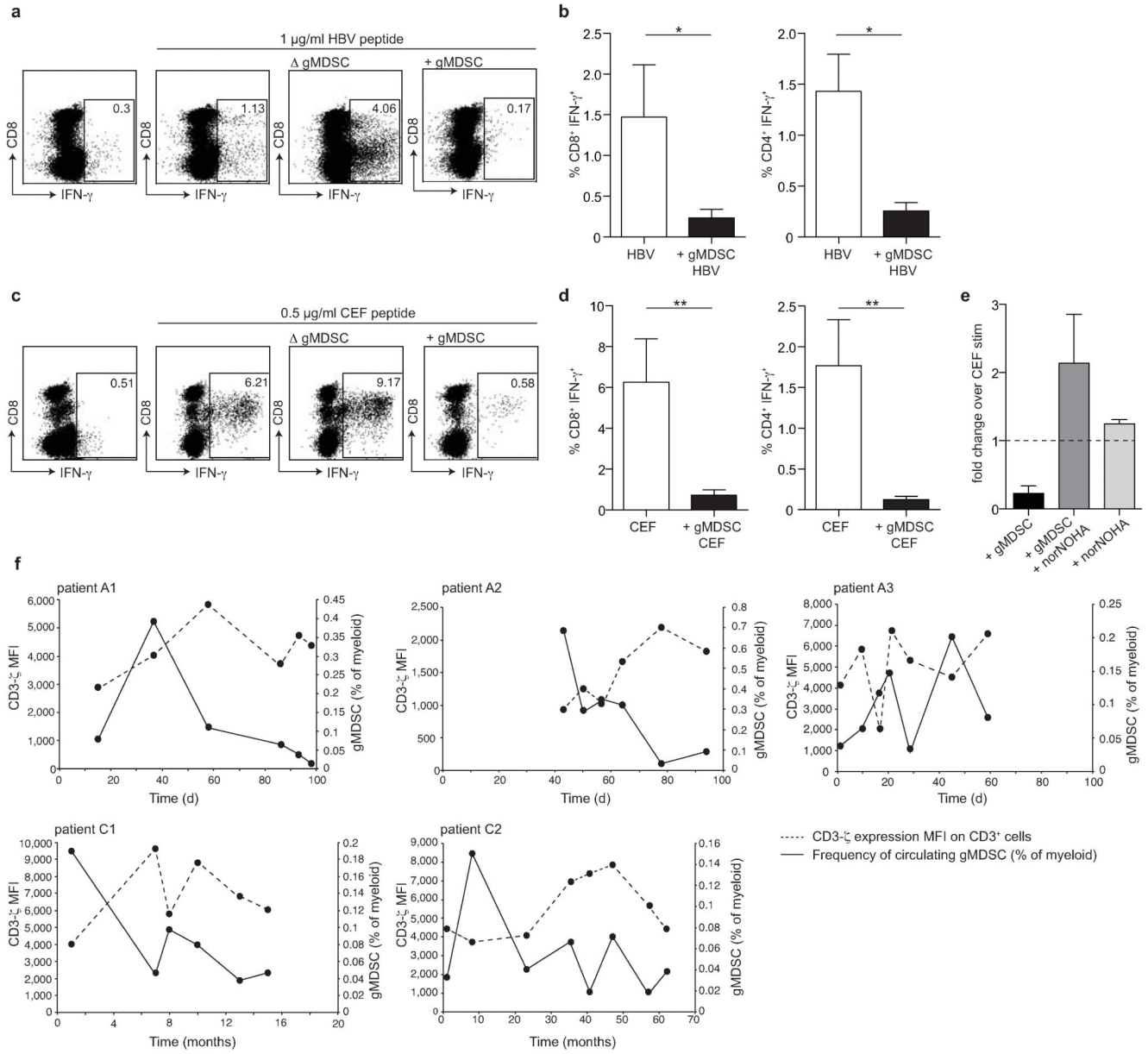

Figure 5. gMDSC suppress functional T cells in an arginase-1 dependent manner

gMDSC were enriched or depleted using sequential magnetic bead isolation ($CD14^{-}CD15^{+}$) from PBMC for direct co-culture with autologous PBMC. gMDSC–enriched (+ gMDSC), depleted (Δ gMDSC), or undepleted PBMC were cultured with 20 IU/ml recombinant IL-2 for 5 days and stimulated to test T cell responses by intracellular cytokine production following peptide stimulation. **a**) Representative FACS plots showing the IFN-γ T cell response with or without stimulation with 1 μg/ml overlapping peptides spanning the core region of HBV genotype D, after gMDSC depletion or enrichment at day 0. **b**) Cumulative data depicting HBV-specific $CD8^{+}$ and $CD4^{+}$ T cell responses (subtraction of background in the absence of stimulation) in PBMC ± gMDSC (n=7, CHB). **c**) Representative FACS plots and **d**) cumulative data for IFN-γ^{+} $CD8^{+}$ and $CD4^{+}$ T cell responses to 0.5 μg/ml CEF-

Europe PMC Funders Author Manuscripts

specific peptide stimulation (minus background as before) in PBMC ± gMDSC (n=18, CHB). Error bars represent the mean ± SEM for the cohorts indicated; * $p<0.05$, ** $p<0.01$; **b, d** paired *t* test. **e**) Fold change $CD8^+$ IFN-γ^- response to CEF peptide in PBMC or gMDSC enriched cultures in the presence or absence of arginase I specific inhibitor nor-NOHA (n=3, CHB). Dotted line indicates response of $CD8^+$ T cells without gMDSC enrichment or nor-NOHA. **f**) MFI of CD3-ζ on $CD3\varepsilon^+$ T cells (dashed line) in relation to circulating gMDSC frequencies as a percentage of myeloid cells (solid line) at multiple time points throughout acute HBV infection (n=3, upper panel) and spontaneous hepatic flares of $HBeAg^-$ CHB (n=2, lower panel).

Europe PMC Funders Author Manuscripts

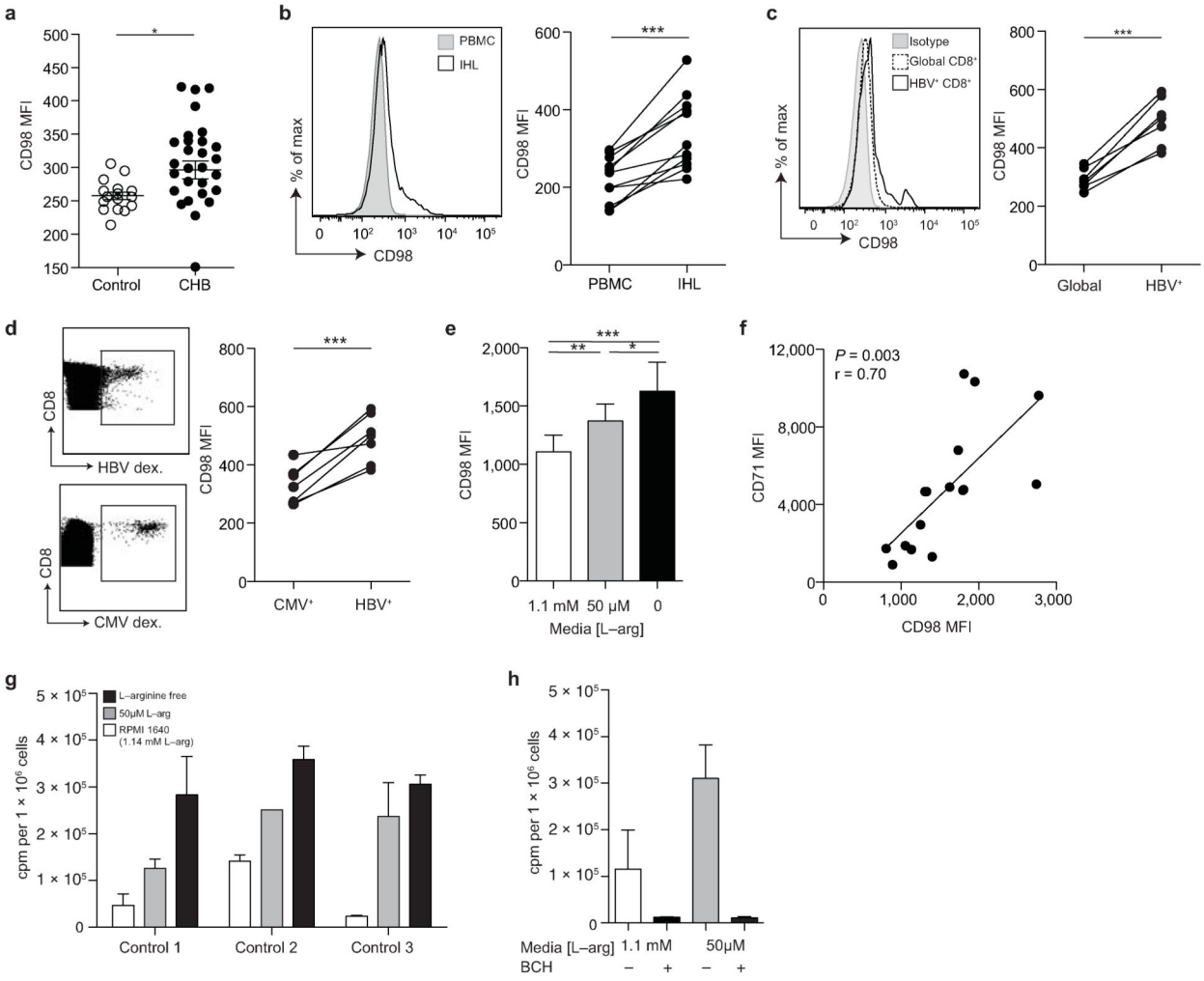

Figure 6. Differential CD98 expression on T cells in CHB

a) Cumulative data depicting expression (MFI) of CD98 on $CD3^+$ T cells (n=15, healthy controls; n=27, CHB). **b**) Representative histogram showing CD98 MFI on peripheral $CD3^+$ (PBMC) and intrahepatic $CD3^+$ (IHL) from a subject with CHB, and the cumulative paired data (n=11, CHB). **c**) Representative histogram showing CD98 MFI on global and HBV-specific $CD8^+$ T cells (identified by e*x vivo* staining with a panel of HLA-A2/HBV peptide dextramers) and the cumulative data (n=7, CHB). **d**) Representative example of identification of paired HBV– and CMV-specific $CD8^+$ T cells using the relevant HLA-A2 dextramers and comparison of their CD98 MFI *ex vivo* (n=7, CHB). **e**) Cumulative data showing CD98 MFI on $CD3^+$ T cells post TCR stimulation (anti-CD3, anti-CD28) for 3 days in cRPMI with a further 24 hr in the presence of 1.14 mM L-arginine (concentration in RPMI1640), 50 μM L-arginine, or in the absence of L-arginine (L-arginine free) (n=20, healthy controls). **f**) Co-expression of CD71 and CD98 on $CD3^+$ T cells in the absence of L-arginine for 24 hr post TCR stimulation (n=15, healthy controls). **g**) Uptake of radiolabelled amino acid (phenylalanine) in T cells post TCR stimulation, before culture varying concentrations of L-arginine for 24 hr. **h**) Radiolabelled phenylalanine uptake in the presence or absence of the system-L inhibitor BCH (10 mM) ± L-arginine deprivation (n=3,

Europe PMC Funders Author Manuscripts

healthy controls). Error bars represent the mean ± SEM for the cohorts indicated; * p<0.05; ** p<0.01; *** p<0.001; **a, e** unpaired *t* test, **b-d** paired *t* test, **f** Pearson product-moment correlation coefficient.

Europe PMC Funders Author Manuscripts